SCIENCE CHINA Materials ARTICLES

mater.scichina.com link.springer.com

Published online 29 August 2017 | doi: 10.1007/s40843-017-9078-1
Sci China Mater 2017, 60(9): 829–838

Enhanced performance of solar cells *via* anchoring $CuGaS_2$ quantum dots

Jinjin Zhao[1,2,3†*], Zhenghao Liu[1,3†], Hao Tang[4], Chunmei Jia[1], Xingyu Zhao[1], Feng Xue[5], Liyu Wei[1,3], Guoli Kong[1], Chen Wang[1] and Jinxi Liu[1*]

ABSTRACT **Ternary I–III–VI quantum dots (QDs) of chalcopyrite semiconductors exhibit excellent optical properties in solar cells. In this study, ternary chalcopyrite $CuGaS_2$ nanocrystals (2–5 nm) were one-pot anchored on TiO_2 nanoparticles (TiO_2@CGS) without any long ligand. The solar cell with TiO_2@$CuGaS_2$/N719 has a power conversion efficiency of 7.4%, which is 23% higher than that of monosensitized dye solar cell. Anchoring $CuGaS_2$ QDs on semiconductor nanoparticles to form QDs/dye co-sensitized solar cells is a promising and feasible approach to enhance light absorption, charge carrier generation as well as to facilitate electron injection comparing to conventional mono-dye sensitized solar cells.**

Keywords: $CuGaS_2$, quantum dots, TiO_2 nanoparticles, solar cells, photo-anode

INTRODUCTION

Quantum-dot-sensitized solar cells (QDSSCs) have gained more attention as a promising option for next-generation solar cells [1–5] due to the quantum confinement effect [6], large dipole moment, high molar coefficients, multiple-exciton generation (MEG), low cost and facile fabrication [7–12]. The chalcopyrite semiconductor quantum dots (QDs), such as CdS(Se) [13–20], PbS(Se) [21–24], $SnSe_2$ [25], InAs [26,27], Sb_2S_3 [28], were introduced into QDSSCs as light-harvesting sensitizers *via* various methods. Since photons with lower energy could be absorbed, the chalcopyrite semiconductor QDs are considered as a promising candidate for the high-efficiency solar cells [29]. The reported semiconductor QDs in QDSSCs were mainly attributed to the binary semiconductor materials. To date, a few ternary semiconductor QDs have been reported in the field of solar cells [30]. Inspired by these researches, the ternary I–III–VI QDs of $A^IB^{III}C_2^{VI}$ (A = Cu, Ag; B = Al, Ga, In; C = S, Se, Te) chalcopyrite semiconductors are expected to exhibit excellent optical properties [31,32]. Recently, some of them have been reported applied on solar cells, such as $CuInS_2$, $CuInSe_2$, $CuInSe_xS_{2-x}$ and $CuIn_xGa_{(1-x)}S_2$ [33–38], which attracted great attention to serve as Pb/Cd-free light-harvesting materials in QDSSCs. Among these ternary semiconductors, $CuGaS_2$ is the most promising ternary compound due to its conductivity, normally p-type [39], large direct band gap energy [40], facile fabrication [38,41], and environmental friendliness. $CuGaS_2$ nanocrystals exhibit excellent activity in solar water splitting [42,43], biological and chemical sensing [44,45]. Ascribing to its wide band gap energy (2.2–2.5 eV) [46,47] corresponding to the green light region and direct transition [29,48–51], $CuGaS_2$ nanocrystals could be an optimum candidate for the QDSSCs. However, very few studies on $CuGaS_2$ QDSSCs were reported. A survey is essential for further experimental efforts in $CuGaS_2$ QDSSCs in order to achieve eco-friendly processes in preparative protocols.

Herein, the $CuGaS_2$ QDs directly and homogeneously grew on TiO_2 nanocrystals (named as TiO_2@CGS) for QDSSCs by a vacuum one-pot nanocasting method. $CuGaS_2$ QDs with particle size of 2–5 nm were anchored on the surface of TiO_2 nanoparticles directly without organic

[1] School of Materials Science and Engineering, Department of Engineering Mechanics, Shijiazhuang Tiedao University, Shijiazhuang 050043, China
[2] Engineering Research Center of Nano-Geo Materials of Ministry of Education, China University of Geosciences, Wuhan 430074, China
[3] Shenzhen Key Laboratory of Nanobiomechanics, Shenzhen Institutes of Advanced Technology, Chinese Academy of Sciences, Shenzhen 518055, China
[4] Department of Materials Science and Engineering, University of Washington, Seattle, WA 98195-2120, USA
[5] Hesteel Group Technology Research Institute, Shijiazhuang 050000, China
[†] These authors contributed equally to this work.
[*] Corresponding authors (emails: jinjinzhao2012@163.com (Zhao J); liujx02@hotmail.com (Liu J))

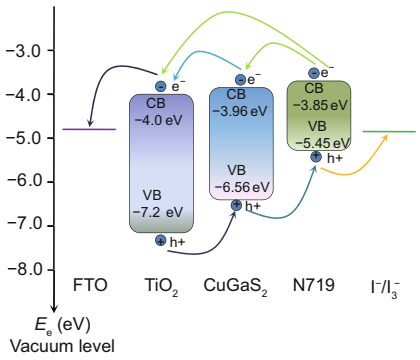

Figure 1 A schematic illustration of the relative band energy levels for charge transfer in the FTO/TiO_2/CGS/N719 electrolyte. *E*)

linker molecules. The relative band energy levels for holes and electrons transfer in the FTO/TiO_2/CGS/N719 electrolyte based QDSSCs are illustrated in Fig. 1. Because of the quantum confinement effects, the $CuGaS_2$ QDs hold a higher conduction band (CB) edge, which facilitates the photoelectron injection from the excited $CuGaS_2$ QDs into TiO_2 nanoparticles [52–54]. Moreover, the $CuGaS_2$ QDs in the TiO_2@CGS nanocrystals could act as complimentary sensitizers to enhance the light harvesting properties in dye sensitized solar cell (DSSC).

EXPERIMENTAL SECTION

Chemicals

Copper chloride ($CuCl_2$), sodium sulfide, titanium tetrachloride (99.5%), ethanol (98%), nitric acid (65%) were bought from Sinopharm Chemical Reagent Co., Ltd; F127 (CAS No. 9003-11-6) was purchased from Sigma-Aldrich, Inc. Polyethylene glycol (PEG; 20000 in molecular weight) and gallium(III) chloride ($GaCl_3$) were purchased from J&K. The sensitizer N719 (*cis*-di(thiocyanato)-*N*,*N*-bis(2, 2′-bipyridyl-4,4′-dicarboxylate)Ru (II)bis-tetrabuty lammonium) electrolyte, surlyn film were purchased from Yingkou Opvtech New Energy Co., Ltd.

Synthesis of the TiO_2@CGS film and fabrication of device

Synthesis of TiO_2 nanoparticles

The synthesis of TiO_2 nanoparticles was as the following procedure [54]. 2.97 g F127 was dissolved in 36.88 g ethanol at 40°C and stirred for 30 min to obtain a clear solution. After that, 3.4 g $TiCl_4$ was added into the prepared clear F127 solution. The precursor solution was then placed into a Teflon-lined stainless steel autoclave (100 mL in capacity) after stirring for 8 h under 40°C. The autoclave was placed in an oven at 160°C for 16 h. Subsequently, the solution was filtered and the products were washed with deionized water and dried at 80°C. Finally, the obtained powders were sintered at 610°C for 10 min after being kept at 300°C for 90 min and 500°C for 240 min. During the entire sintering process, the heating rate was kept at a constant of 2°C min^{-1}. After sintering, the products were dispersed in deionized water and nitric acid (65%) until the pH of this suspension reached to about 2. The suspension was vigorously stirred at 80°C for 8 h to obtain TiO_2 nanoparticles.

Preparation of TiO_2@CGS nanoparticles

TiO_2 nanoparticles were put into a sealed container and subjected to vacuum. After vacuumed for 30 min, the mixed solution of $GaCl_3$ (0.2 mol L^{-1}) was allowed to enter into the vacuum system, and then held for 10 min before the solvent was fully removed by evaporation. The precipitate was dried in vacuum oven at 80°C for 8 h. After drying, the mixed powder was washed twice with ethanol and dried in vacuum oven again. This entire procedure described above was repeated twice except that the $GaCl_3$ solution used was replaced by 0.2 mol L^{-1} $CuCl_2$ aqueous solution and 0.4 mol L^{-1} Na_2S aqueous solution, respectively. Finally, the sample was calcined in Ar gas at 500°C for 1 h to obtain TiO_2@CGS nanoparticles.

Preparation of mesoporous TiO_2 films and TiO_2@CGS film

The mesoporous TiO_2 films were prepared by the doctor-blade method [55]. The TiO_2 paste was made from the TiO_2 nanoparticles synthesized in the previous section. Briefly, 0.8 g TiO_2 was added into a mixed solution of ethanol/deionized water (3:1) and ultrasonicated for 30 min after the addition of PEG aqueous which acted as the pore-forming material. After that, the mixture was grinded into ropiness in agate mortar. A mask, with a window encompassed by 3M scotch tape, was used to define the 5 mm × 5 mm area which was used to spread the paste dropped on edge of the window with a glass slide on the fluorine doped tin oxide (FTO) conductive glass (SnO_2:F coated glass). Subsequently, the as-prepared TiO_2 films were sintered in air with a heating rate of 2°C min^{-1} from room temperature to 300°C for 30 min, and to 500°C for 60 min. The synthesis of mesoporous TiO_2@CGS film was as the same procedure as the one described above.

Fabrication of quantum dot-dye bilayer-sensitized solar cells (QDBSC)

The mesoporous TiO_2 film and TiO_2@CGS film were sensitized with N719 dye by direct adsorption. Firstly, the

as-prepared TiO_2 film and TiO_2@CGS film were heated to 80°C and immersed into the N719 ethanol solution (0.5 mmol L^{-1}) for 24 h. After rinsing the film in solution by ethanol and drying in air, the desired mesoporous TiO_2/N719 film and TiO_2@CGS/N719 electrodes were obtained. The photovoltaic cells were assembled with the mesoporous TiO_2/N719 or TiO_2@CGS/N719 photoelectrode, Pt coated counter electrode, and sealing material (OPV-SN-60) with a thickness of 60 μm. Commercially available electrolyte of I_3^-/I^- was injected into the space between the photoelectrode and the counter electrode.

Characterization

X-ray diffraction (XRD) patterns of powders were obtained using D8 Advance (Germany) diffractometer with Cu Kα radiation (40 kV and 40 mA) with a scanning rate of 4° min^{-1} for wide angle tests. The N_2 sorption measurements were performed by using Micromeritics Tristar 3000 for mesoporosity and Micromeritics ASAP 2020 for porosimeters and microporosity at 77 K, respectively. The mesoporous specific surface area and the pore size distribution were calculated using the Brunauer–Emmett–Teller (BET) method. Scanning electron microscopy (SEM) analysis was performed on a Hitachi-S-4800 electron microscope. Transmission electron microscopy (TEM) images were obtained on a JEOL-2010F electron microscope operated at 200 kV. The UV-vis absorbance spectra were measured by a Shimadzu UV-2550 spectrophotometer. Symmetric dummy cells were used for the electrochemical impedance spectroscopy (EIS) measurements. The EIS measurements were conducted by using a computer-controlled electrochemical workstation (CHI660A, Chenhua, Shanghai) in dark. Photovoltaic measurement (*J-V*) was recorded with a Newport Oriel class AAA solar simulator (model 92250A-1000) equipped with a class A 300 W xenon light source powered by a Newport power supply (model 69907). The power output of the lamp was calibrated to 1 Sun (AM1.5G, 100 mW cm^{-2}) using a certified Si reference cell (VLSI standard, S/N 10510-0031). The current-voltage characteristics of each cell were measured with a Keithley-2400 digital source meter. Photovoltaic performance was characterized by using a mask with an aperture area of 0.25 cm^2. The incident photon-to-current efficiency (IPCE) was measured in DC mode with a 1/4 m double monochromator (Crowntech DK242), a multi-meter (Keithley 2000), and two light sources depending on the wavelength range required (300–600 nm: xenon lamp, 300 W; 600–900 nm: tungsten-halogen lamp, 150 W). The monochromatic light intensity for IPCE efficiency was calibrated with a reference silicon photodiode. All the measurements were conducted under ambient conditions.

RESULTS AND DISCUSSION

To characterize the phase structures and crystal size, the XRD pattern of the TiO_2@$CuGaS_2$ nanoparticles is shown in Fig. 2, which well matches with that of anatase phase TiO_2 (JCPDS 21-1272) and $CuGaS_2$. Although some peaks of TiO_2 and $CuGaS_2$ were seen overlapped, the XRD of $CuGaS_2$ exhibited several diffraction peaks in consistent with 2θ values of 29.12°, 48.07°, 48.60°, 57.17°, 58.15°, and 70.36°, and these peaks can be attributed to (112), (220), (204), (312), (116), and (400) planes of $CuGaS_2$ (JCPDS 25-0279). The XRD diffraction features of TiO_2@$CuGaS_2$ sample indicated the composite materials of anatase TiO_2 and gallite $CuGaS_2$, which conformed well with the electron diffraction patterns of TEM in Fig. 3.

Fig. 3 shows the TEM images of TiO_2@CGS nanocrystals and bare TiO_2 particles. The TEM images of bare TiO_2 nanoparticles in Fig. 3a and the synthesized TiO_2@CGS nanocrystals in Fig. S1 and Fig. 3b show that the diameter of the prepared TiO_2 particles is about 20–50 nm, and the $CuGaS_2$ QDs have an average size of approximately 2–5 nm. The high resolution TEM images in Fig. 3c exhibit the crystalline structure of the synthesized $CuGaS_2$ QDs. Fig. 3d is the spectra taken *via* energy-dispersive spectroscopy (EDS) for TiO_2@CGS nanocrystals, which shows the existence of Cu, Ga, S elements in the QDs with the ratio of Cu/Ga/S to be 1.04 (±0.1):1.0:1.90(±0.2). SEM-EDS mapping of TiO_2@CGS nanocrystals is shown in Fig. 4 to characterize the elemental distribution. The molar ratio of $CuGaS_2$ in TiO_2@CGS could be determined to be 5.4% by EDS analysis and the QDs are off-stoichiometric $CuGaS_2$ with a uniform elemental distribution.

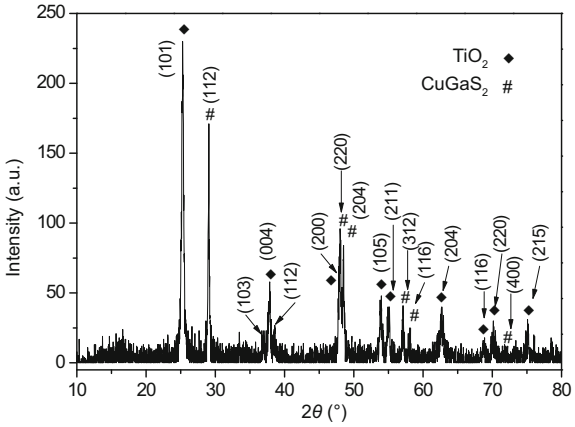

Figure 2 XRD pattern of the TiO_2@CGS nanoparticles.

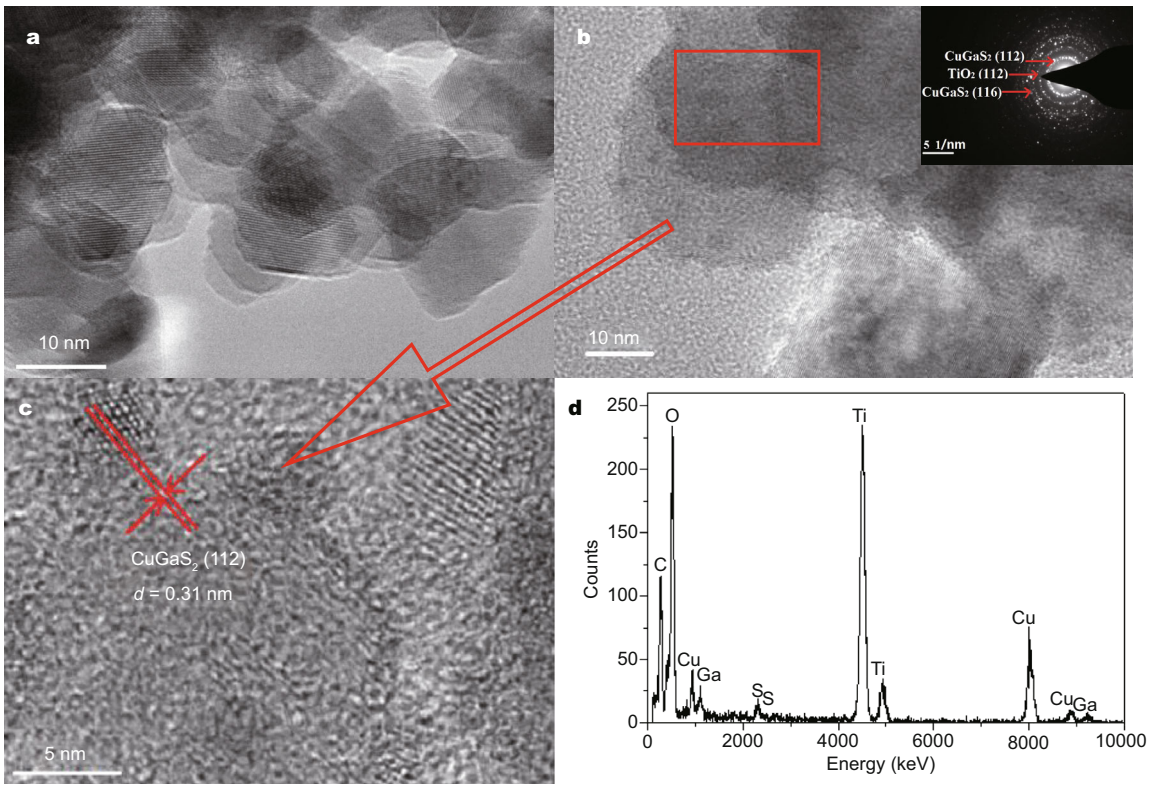

Figure 3 TEM images of (a) TiO_2 nanoparticles and (b) the synthesized TiO_2@CGS nanocrystals. Inset of (b) is the selected-area electron diffraction pattern of TiO_2@CGS. (c) HR-TEM image of TiO_2@CGS taken from the area within red square in (b). (d) Simultaneous EDS spectra of TiO_2@CGS.

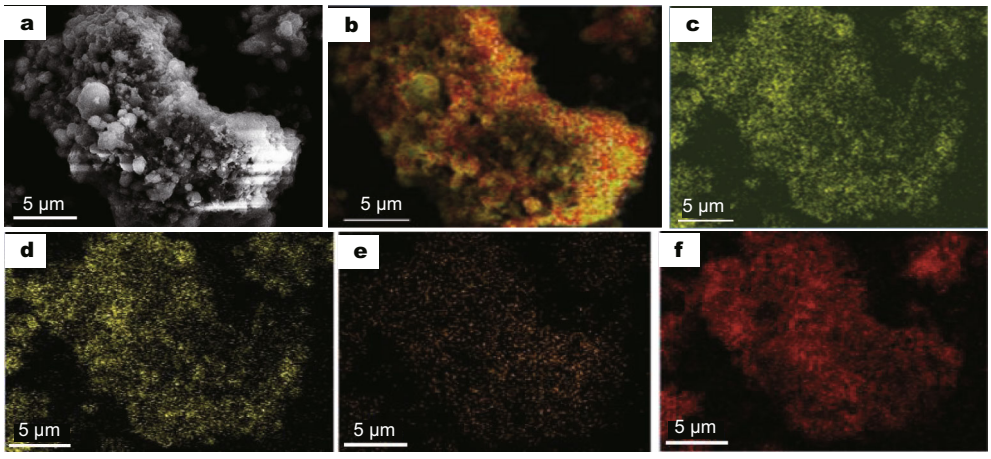

Figure 4 SEM images (a) and (b) of TiO_2@CGS; SEM-EDS elemental mapping of (c) Ti, (d) Cu, (e) Ga and (f) S.

Fig. 5 shows the N_2 adsorption-desorption isotherms measured for TiO_2@CGS nanoparticles and naked TiO_2 to characterize their specific surface areas and pore volumes. Both isotherms of TiO_2@CGS and TiO_2 nanoparticles exhibit hysteresis loops of type-H1, with the adsorption and desorption jumps at 0.6 and 1.0, which is characteristic for mesoporous materials. According to the Barrett-Joyner-Halenda (BJH) method and derived from the desorption branch shown in Fig. 5 and Table 1, the pore size distribution of TiO_2@CGS shows a smaller mesopore size of 3.6 nm compared to 10.4 nm of TiO_2 nanoparticles. The BET surface area and mesopore volume of TiO_2@CGS are measured to be 22.03 $m^2 g^{-1}$ and 0.098 $cm^3 g^{-1}$, respectively, which are 51.3% and 40.2%

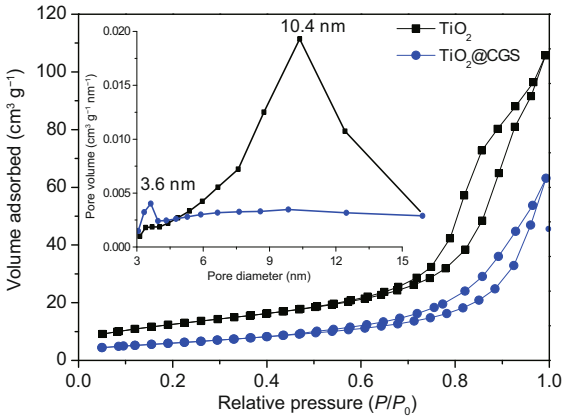

Figure 5 N_2 adsorption–desorption isotherms and the corresponding pore diameter distribution curves of different samples (inset).

less than those of TiO_2 nanoparticles, in accordance with previously reported studies [54]. Smaller particle size (2–5 nm) of the CGS QDs led to a severe aggregation within the mesopores, and thus decreased the mesopore volume. Due to the larger density of CGS QDs, even with an increased surface area, the specific surface area calculated *via* BET method got reduced. Whereas, the decreased BET surface area and mesopore volume of TiO_2@CGS are still good enough to enrich the loading capacity of the N719 dye [55].

Fig. 6a shows the UV-vis absorption spectra of bare TiO_2 film and the TiO_2@CGS film before and after sensitized with N719. The absorption onset for TiO_2 film is shorter than 400 nm, which is in the region of ultraviolet. TiO_2 film with CGS could absorb light with wavelength shorter than 530 nm, and the two absorption peaks of N719 dye are at 430 and 520 nm, respectively. By sensitizing $CuGaS_2$ QDs in TiO_2/N719, the absorption spectra of the TiO_2@CGS/N719 films got a significant red-shift and extended to around 700 nm. Fig. 6b shows the plots of $(Ahv)^2$ *versus* hv (A = absorbance, h = Planck's constant, and v = frequency) for all samples, from which it is possible to extrapolate the slope near the absorption onset and to extract the energy of band gap. The curves yielded band gaps of 2.69 eV for TiO_2@CGS, 2.25 eV for TiO_2/N719, and 2.03 eV for TiO_2@CGS/N719, respectively. Thus, the introduction of sensitized $CuGaS_2$ QDs could enhance the light harvesting ability in TiO_2/N719, which can be attributed to the following factors: a higher intensity and a red shift of light absorption edge from 600 nm to around 700 nm. Such improvement could lead to an increased electron concentration in TiO_2/N719 substrate sensitized with $CuGaS_2$ QDs [56–62].

Co-sensitization of semiconductor QDs and organic dyes has also been investigated as an effective strategy for enrichment [54,55,63,64]. The *J-V* curves in Fig. 7 shows that these two absorbers also have vital contributions on the overall cell performance. The bisensitized device (TiO_2@CGS/N719) is revealed to have a great improvement on its photovoltaic performance, compared to the one with monosensitizers. Table 2 lists the open circuit potential (V_{oc}), short circuit current density (J_{sc}), fill factor

Table 1 Structural parameters of TiO_2 nanoparticles and TiO_2@CGS

	BET surface area ($m^2\ g^{-1}$)	Mesopore volume ($cm^3\ g^{-1}$)	Mesopore size (nm)
TiO_2@CGS	22.03	0.098	3.6
TiO_2	45.24	0.164	10.4

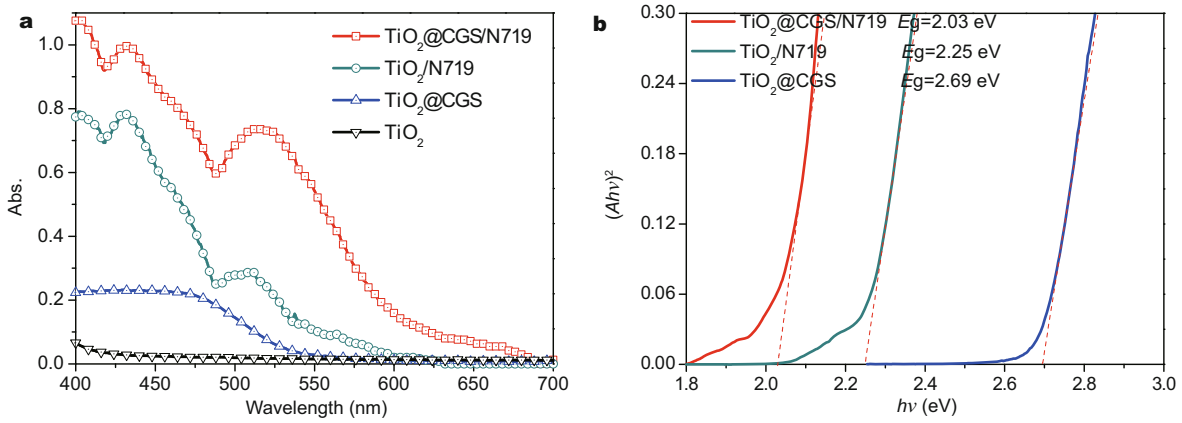

Figure 6 (a) UV-vis absorption spectra of different samples; (b) plots of $(Ahv)^2$ against the photon.

(FF) and total energy conversion efficiency (η) of these devices. The V_{oc} increased from 704 to 756 mV (+52 mV) and J_{sc} increased from 14.88 to 18.36 mA cm^{-2} (+23.4%) after co-sensitized with CGS. However, FF reduced from 0.572 to 0.53, mainly owing to increased charge carrier recombination rate and larger shunt resistance indicated by the slope of J_{sc} point of the *J-V* curve. Consequently, in one sun illumination condition, η of the bisensitized device with TiO_2@CGS/N719 as photoanode could reach up to 7.4%, which is 23% higher than that with TiO_2@N719 [61,62].

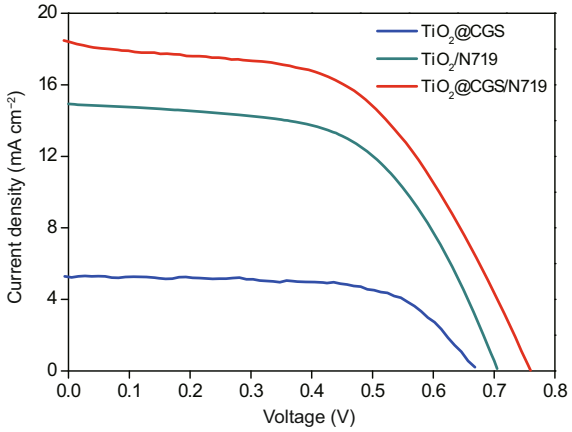

Figure 7 Photocurrent density–voltage characteristic curves of different solar cells.

Attributed to the red-shift visual light absorption, TiO_2@CGS/N719 co-sensitized solar cell displays a higher energy conversion efficiency. The IPCE spectra shown in Fig. 8 investigate the role of $CuGaS_2$ quantum dots. The trend of the IPCE spectra of TiO_2@CGS/N719 co-sensitized solar cell and TiO_2/N719 dye sensitized solar cell are in accordance with that of UV-vis absorption spectra. The calculated J_{sc} values of TiO_2@CGS/N719, TiO_2/N719, TiO_2@CGS devices are 18.1, 14.2, and 5.0 mA cm^{-2}, respectively, in consistent with the *J-V* curves. By introducing the $CuGaS_2$ QDs as a co-sensitizer, the photon-to-electron conversion efficiency got significantly enhanced.

To investigate the effects of QDs on charge transport and recombination at the photoanode, EIS under dark was carried out to exhibit the representative impedance plots of cells based on TiO_2@CGS, TiO_2/N719 and TiO_2@CGS/N719 photoanodes, shown in Fig. 9. The equivalent circuit in Fig. 9 is used to fit the impedance measurements, which is composed of resistance-capacitance pairs and a distributed element to describe redefinable characteristics of the electrode and its interfaces with the electrolyte [65]. The resistance R records recombination in the solar cell, while C relates to the carrier accumulation and splitting of thΩe Fermi levels [66]. The main semicircle in Fig. 9 is relevant to the charge transfer process at the interface of anode-electrolyte. The frequency large arcs (the semicircles from 32 to 160 Ω) are

Table 2 Photovoltaic parameters of different solar cells

	V_{oc} (mV)	J_{sc} (mA cm^{-2})	FF	η (%)
TiO_2@CGS/N719	756	18.36	0.53	7.4
TiO_2@CGS	672	5.26	0.649	2.29
TiO_2/N719	704	14.88	0.572	6

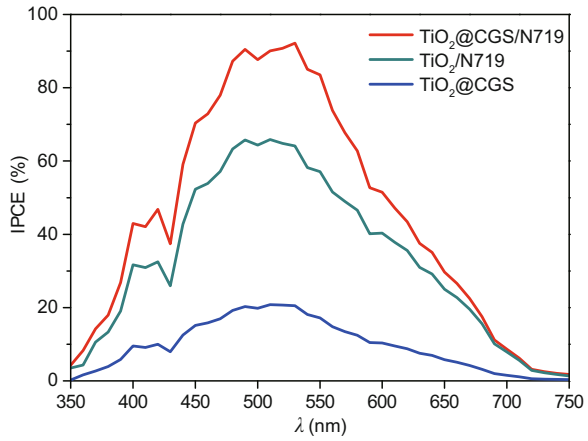

Figure 8 IPCE spectra of the solar cells fabricated with different photoanodes.

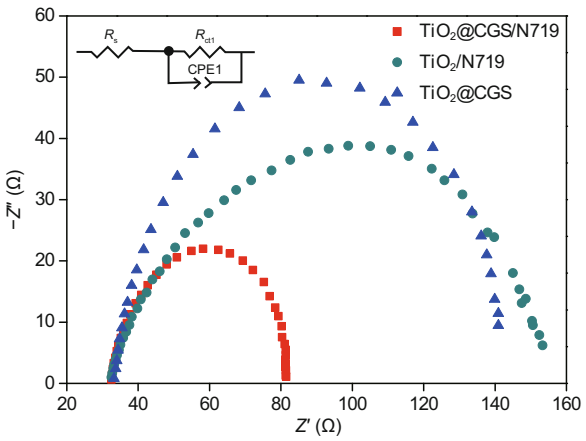

Figure 9 Impedance spectra and the inset is the corresponding equivalent circuit.

ascribed to the anode/electrolyte interfacial charge transfer resistance or recombination (R_{ct1}) in parallel with the capacitance (CPE_1) in the TiO_2-based anodes and the anodes/electrolyte interface. The diameter of the semicircle exhibits the charge transfer resistance (recombination) at the anodes/electrolyte interfaces [8,67,68]. Obviously, comparing devices with TiO_2@CGS/N719 and TiO_2/N719 as photoanodes, the TiO_2@CGS/N719 based cell has a smaller diameter of the semicircle, which exhibits a decreased charge recombination resistance and a certain portion of the injected charges are lost by electron transfer from TiO_2 to I_3^- in the electrolyte. Meanwhile, the TiO_2@CGS/N719 photoanode with doped CGS QDs and dye shell decreased the direct contact surface area between bare TiO_2 surface and the electrolyte, which reduced the charge recombination resistance.

CONCLUSIONS

Novel visible-light induced TiO_2@$CuGaS_2$ nanocrystals have been successfully synthesized *via* the vacuum one-pot-nanocasting process, with $CuGaS_2$ (2–5 nm) grown uniformly on TiO_2 (20–50 nm). The TiO_2@$CuGaS_2$/N719 photoanode shows an excellent absorbance on broad wavelength light due to the narrow energy band gap (E_g = 2.03 eV). Photoanodes with the TiO_2 and TiO_2@$CuGaS_2$ nanocrystals were fabricated and the device with TiO_2@$CuGaS_2$/N719 has a power conversion efficiency η of 7.4%, which is 23% higher than that of monosensitized dye solar cell. Anchoring $CuGaS_2$ QDs on semiconductor nanoparticles to form QDs/dye co-sensitized solar cells is a promising and feasible approach to enhance light absorption, charge carrier generation as well as to facilitate electron injection comparing to conventional dye sensitized solar cells.

Received 23 May 2017; accepted 15 July 2017; published online 29 August 2017

1 Kamat PV. Quantum dot solar cells. Semiconductor nanocrystals as light harvesters. J Phys Chem C, 2008, 112: 18737–18753
2 Nozik AJ. Quantum dot solar cells. Phys E-Low-dimensional Syst Nanostruct, 2002, 14: 115–120
3 Sargent EH. Colloidal quantum dot solar cells. Nat Photon, 2012, 6: 133–135
4 Zhao H, Wu Q, Hou J, *et al.* Enhanced light harvesting and electron collection in quantum dot sensitized solar cells by TiO_2 passivation on ZnO nanorod arrays. Sci China Mater, 2017, 60: 239–250
5 Ren F, Li S, He C. Electrolyte for quantum dot-sensitized solar cells assessed with cyclic voltammetry. Sci China Mater, 2015, 58: 490–495
6 Grätzel M. Dye-sensitized solar cells. J Photochem PhotoBiol C-Photochem Rev, 2003, 4: 145–153
7 Chang JY, Chang SC, Tzing SH, *et al.* Development of non-stoichiometric $CuInS_2$ as a light-harvesting photoanode and catalytic photocathode in a sensitized solar cell. ACS Appl Mater Interfaces, 2014, 6: 22272–22281
8 Huang X, Huang S, Zhang Q, *et al.* A flexible photoelectrode for CdS/CdSe quantum dot-sensitized solar cells (QDSSCs). Chem Commun, 2011, 47: 2664–2666
9 Kim MR, Ma D. Quantum-dot-based solar cells: recent advances, strategies, and challenges. J Phys Chem Lett, 2015, 6: 85–99
10 Zheng X, Yu D, Xiong FQ, *et al.* Controlled growth of semiconductor nanofilms within TiO_2 nanotubes for nanofilm sensitized solar cells. Chem Commun, 2014, 50: 4364–4367
11 Coughlan C, Ibáñez M, Dobrozhan O, *et al.* Compound copper chalcogenide nanocrystals. Chem Rev, 2017, 117: 5865–6109
12 Tian J, Cao G. Control of nanostructures and interfaces of metal oxide semiconductors for quantum-dots-sensitized solar cells. J Phys Chem Lett, 2015, 6: 1859–1869
13 Hossain MA, Jennings JR, Koh ZY, *et al.* Carrier generation and collection in CdS/CdSe-sensitized SnO_2 solar cells exhibiting unprecedented photocurrent densities. ACS Nano, 2011, 5: 3172–3181
14 Kongkanand A, Tvrdy K, Takechi K, *et al.* Quantum dot solar cells. Tuning photoresponse through size and shape control of CdSe–TiO_2 architecture. J Am Chem Soc, 2008, 130: 4007–4015
15 Lee HJ, Bang J, Park J, *et al.* Multilayered semiconductor (CdS/CdSe/ZnS)-sensitized TiO_2 mesoporous solar cells: all prepared by successive ionic layer adsorption and reaction processes. Chem Mater, 2010, 22: 5636–5643
16 Lee YL, Lo YS. highly efficient quantum-dot-sensitized solar cell based on co-sensitization of CdS/CdSe. Adv Funct Mater, 2009, 19: 604–609
17 Ren S, Chang LY, Lim SK, *et al.* Inorganic–organic hybrid solar cell: bridging quantum dots to conjugated polymer nanowires. Nano Lett, 2011, 11: 3998–4002
18 Robel I, Subramanian V, Kuno M, *et al.* Quantum dot solar cells. Harvesting light energy with cdse nanocrystals molecularly linked to mesoscopic TiO_2 films. J Am Chem Soc, 2006, 128: 2385–2393
19 Santra PK, Kamat PV. Mn-doped quantum dot sensitized solar cells: a strategy to boost efficiency over 5%. J Am Chem Soc, 2012, 134: 2508–2511
20 Santra PK, Kamat PV. Tandem-layered quantum dot solar cells: tuning the photovoltaic response with luminescent ternary cadmium chalcogenides. J Am Chem Soc, 2013, 135: 877–885
21 Guijarro N, Lana-Villarreal T, Lutz T, *et al.* Sensitization of TiO_2 with PbSe quantum dots by SILAR: how mercaptophenol improves charge separation. J Phys Chem Lett, 2012, 3: 3367–3372
22 Luther JM, Gao J, Lloyd MT, *et al.* Stability assessment on a 3% bilayer PbS/ZnO quantum dot heterojunction solar cell. Adv Mater, 2010, 22: 3704–3707
23 Parsi Benehkohal N, González-Pedro V, Boix PP, *et al.* Colloidal PbS and PbSeS quantum dot sensitized solar cells prepared by electrophoretic deposition. J Phys Chem C, 2012, 116: 16391–16397
24 Tian J, Shen T, Liu X, *et al.* Enhanced performance of PbS-quantum-dot-sensitized Solar cells *via* optimizing precursor solution and electrolytes. Sci Rep, 2016, 6: 23094
25 Yu X, Zhu J, Zhang Y, *et al.* $SnSe_2$ quantum dot sensitized solar cells prepared employing molecular metal chalcogenide as precursors. Chem Commun, 2012, 48: 3324–3326

26 Guimard D, Morihara R, Bordel D, *et al.* Fabrication of InAs/GaAs quantum dot solar cells with enhanced photocurrent and without degradation of open circuit voltage. Appl Phys Lett, 2010, 96: 203507
27 Yu P, Zhu K, Norman AG, *et al.* Nanocrystalline TiO_2 solar cells sensitized with InAs quantum dots. J Phys Chem B, 2006, 110: 25451–25454
28 Heo JH, Im SH, Kim H, *et al.* Sb_2S_3-sensitized photoelectrochemical cells: open circuit voltage enhancement through the introduction of poly-3-hexylthiophene interlayer. J Phys Chem C, 2012, 116: 20717–20721
29 Lv X, Yang S, Li M, *et al.* Investigation of a novel intermediate band photovoltaic material with wide spectrum solar absorption based on Ti-substituted $CuGaS_2$. Sol Energ, 2014, 103: 480–487
30 Nozik AJ, Beard MC, Luther JM, *et al.* Semiconductor quantum dots and quantum dot arrays and applications of multiple exciton generation to third-generation photovoltaic solar cells. Chem Rev, 2010, 110: 6873–6890
31 Hamanaka Y, Ogawa T, Tsuzuki M, *et al.* Photoluminescence properties and its origin of $AgInS_2$ quantum dots with chalcopyrite structure. J Phys Chem C, 2011, 115: 1786–1792
32 Omata T, Nose K, Otsuka-Yao-Matsuo S. Size dependent optical band gap of ternary I-III-VI2 semiconductor nanocrystals. J Appl Phys, 2009, 105: 073106–073106
33 Allen PM, Bawendi MG. Ternary I−III−VI quantum dots luminescent in the red to near-infrared. J Am Chem Soc, 2008, 130: 9240–9241
34 Feng J, Han J, Zhao X. Synthesis of $CuInS_2$ quantum dots on TiO_2 porous films by solvothermal method for absorption layer of solar cells. Prog Org Coatings, 2009, 64: 268–273
35 Li L, Daou TJ, Texier I, *et al.* Highly luminescent $CuInS_2$/ZnS core/shell nanocrystals: cadmium-free quantum dots for *in vivo* imaging. Chem Mater, 2009, 21: 2422–2429
36 Norako ME, Brutchey RL. Synthesis of metastable wurtzite cuInSe$_2$ nanocrystals. Chem Mater, 2010, 22: 1613–1615
37 Singh A, Coughlan C, Laffir F, *et al.* Assembly of $CuIn_{1-x}Ga_xS_2$ nanorods into highly ordered 2D and 3D superstructures. ACS Nano, 2012, 6: 6977–6983
38 Chang SH, Chiu BC, Gao TL, *et al.* Selective synthesis of copper gallium sulfide ($CuGaS_2$) nanostructures of different sizes, crystal phases, and morphologies. CrystEngComm, 2014, 16: 3323–3330
39 Wagner S, Shay JL, Tell B, *et al.* Green electroluminescence from CdS–$CuGaS_2$ heterodiodes. Appl Phys Lett, 1973, 22: 351–353
40 Tung HT, Hwu Y, Chen IG, *et al.* Fabrication of single crystal $CuGaS_2$ nanorods by X-ray irradiation. Chem Commun, 2011, 47: 9152–9154
41 Vahidshad Y, Mirkazemi SM, Tahir MN, *et al.* Facile one-pot synthesis of polytypic (wurtzite–chalcopyrite) $CuGaS_2$. Appl Phys A, 2016, 122: 187
42 Kandiel TA, Anjum DH, Sautet P, *et al.* Electronic structure and photocatalytic activity of wurtzite Cu–Ga–S nanocrystals and their Zn substitution. J Mater Chem A, 2015, 3: 8896–8904
43 Zhao M, Huang F, Lin H, *et al.* $CuGaS_2$–ZnS p–n nanoheterostructures: a promising visible light photo-catalyst for water-splitting hydrogen production. Nanoscale, 2016, 8: 16670–16676
44 Zhou Q, Kang SZ, Li X, *et al.* One-pot hydrothermal preparation of wurtzite $CuGaS_2$ and its application as a photoluminescent probe for trace detection of l-noradrenaline. Colloids Surfs A-PhysicoChem Eng Aspects, 2015, 465: 124–129
45 Zhou Q, Kang SZ, Li X, *et al.* A facile self-assembled film assisted preparation of $CuGaS_2$ ultrathin films and their high sensitivity to L-noradrenaline. Appl Surf Sci, 2016, 363: 659–663
46 Liu Z, Hao Q, Tang R, *et al.* Facile one-pot synthesis of polytypic $CuGaS_2$ nanoplates. Nanoscale Res Lett, 2013, 8: 524
47 Tell B, Shay JL, Kasper HM. Room-temperature electrical properties of ten I-III-VI_2 semiconductors. J Appl Phys, 1972, 43: 2469–2470
48 Han M, Zhang X, Zeng Z. The investigation of transition metal doped $CuGaS_2$ for promising intermediate band materials. RSC Adv, 2014, 4: 62380–62386
49 Shay JL, Wernick JH. Ternary Chalcopyrite Semiconductors, Growth, Electronic properties, and applications. Oxford: Pergramon Press, 1975
50 Xiao N, Zhu L, Wang K, *et al.* Synthesis and high-pressure transformation of metastable wurtzite-structured $CuGaS_2$ nanocrystals. Nanoscale, 2012, 4: 7443–7447
51 Regulacio MD, Ye C, Lim SH, *et al.* Facile noninjection synthesis and photocatalytic properties of wurtzite-phase $CuGaS_2$ nanocrystals with elongated morphologies. CrystEngComm, 2013, 15: 5214–5217
52 Li TL, Lee YL, Teng H. $CuInS_2$ quantum dots coated with CdS as high-performance sensitizers for TiO_2 electrodes in photoelectrochemical cells. J Mater Chem, 2011, 21: 5089–5098
53 Li TL, Lee YL, Teng H. High-performance quantum dot-sensitized solar cells based on sensitization with $CuInS_2$ quantum dots/CdS heterostructure. Energ Environ Sci, 2012, 5: 5315–5324
54 Zhao J, Zhang J, Wang W, *et al.* Facile synthesis of $CuInGaS_2$ quantum dot nanoparticles for bilayer-sensitized solar cells. Dalton Trans, 2014, 43: 16588–16592
55 Wang X, Wang P, Dong Z, *et al.* Highly sensitive fluorescence probe based on functional SBA-15 for selective detection of Hg^{2+}. Nanoscale Res Lett, 2010, 5: 1468–1473
56 Alonso MI, Wakita K, Pascual J, *et al.* Optical functions and electronic structure of $CuInSe_2$, $CuGaSe_2$, $CuInS_2$, and $CuGaS_2$. Phys Rev B, 2001, 63: 075203
57 Yang L, McCue C, Zhang Q, *et al.* Highly efficient quantum dot-sensitized TiO_2 solar cells based on multilayered semiconductors (ZnSe/CdS/CdSe). Nanoscale, 2015, 7: 3173–3180
58 Chen S, Gong XG, Walsh A, *et al.* Crystal and electronic band structure of Cu_2ZnSnX_4 (X=S and Se) photovoltaic absorbers: first-principles insights. Appl Phys Lett, 2009, 94: 041903
59 Jaffe JE, Zunger A. Theory of the band-gap anomaly in ABC_2 chalcopyrite semiconductors. Phys Rev B, 1984, 29: 1882–1906
60 Nie X, Wei SH, Zhang SB. Bipolar doping and band-gap anomalies in delafossite transparent conductive oxides. Phys Rev Lett, 2002, 88: 066405
61 Tell B, Shay JL, Kasper HM. Electrical properties, optical properties, and band structure of $CuGaS_2$ and $CuInS_2$. Phys Rev B, 1971, 4: 2463–2471
62 Ju T, Graham RL, Zhai G, *et al.* High efficiency mesoporous titanium oxide PbS quantum dot solar cells at low temperature. Appl Phys Lett, 2010, 97: 043106
63 Chen L, Huang R, Ma YJ, *et al.* Controllable synthesis of hollow and porous Ag/$BiVO_4$ composites with enhanced visible-light photocatalytic performance. RSC Adv, 2013, 3: 24354–24361
64 Zhao J, Wang P, Wei L, *et al.* Enhanced photocurrent by the co-sensitization of ZnO with dye and CuInSe nanocrystals. Dalton Trans, 2015, 44: 12516–12521
65 Gonzalez-Pedro V, Xu X, Mora-Sero I, *et al.* Modeling high-efficiency quantum dot sensitized solar cells. ACS Nano, 2010, 4:

5783–5790
66 Fabregat-Santiago F, Garcia-Belmonte G, Mora-Seró I, *et al.* Characterization of nanostructured hybrid and organic solar cells by impedance spectroscopy. Phys Chem Chem Phys, 2011, 13: 9083–9118
67 Mahmood K, Kang HW, Park SB, *et al.* Hydrothermally grown upright-standing nanoporous nanosheets of iodine-doped ZnO (ZnO:I) nanocrystallites for a high-efficiency dye-sensitized solar cell. ACS Appl Mater Interfaces, 2013, 5: 3075–3084
68 Xie Y, Joshi P, Darling SB, *et al.* Electrolyte effects on electron transport and recombination at ZnO nanorods for dye-sensitized solar cells. J Phys Chem C, 2010, 114: 17880–17888

Acknowledgements The authors thank the financial support from the National Key Research and Development Program of China (2016YFA0201001), the National Natural Science Foundation of China (11627801, 51102172 and 11772207), Science and Technology Plan of Shenzhen City (JCYJ20160331191436180), the Leading Talents of Guangdong Province Program (2016LJ06C372), the Natural Science Foundation for Outstanding Young Researcher in Hebei Province (E2016210093), the Key Program of Educational Commission of Hebei Province of China (ZD2016022), the Youth Top-notch Talents Supporting Plan of Hebei Province, the Graduate Innovation Foundation of Shijiazhuang Tiedao University, Hebei Provincial Key Laboratory of Traffic Engineering materials, and Hebei Key Discipline Construction Project.

Author contributions Zhao J and Liu Z designed and engineered the samples; Liu Z, Jia C and Kong G performed the experiments; Xue F and Wei L performed the structural and *J-V* performance measurement; Wang C and Wei L performed the data analysis; Zhao J wrote the paper with support from Liu J and Tang H. All authors contributed to the general discussion.

Conflict of interest The authors declare that they have no conflict of interest.

Supplementary information Supporting materials are available in the online version of the paper.

Jinjin Zhao obtained her BE degree in materials science and engineering from Hebei University of Science and Technology in 2005, and her PhD in materials physics and chemistry from Shanghai Institute of Ceramics, Chinese Academy of Sciences in 2010. She did her visiting doctoral studies at Max Plank Institute of Colloids and Interfaces, Germany, from October 2007 to October 2008, and visiting scholar at the University of Washington from August 2015 to August 2016. She holds faculty appointment in Shijiazhuang Tiedao University. She is interested in probing multi-physical couplings in perovskite solar cells based on dynamic photovoltaic thermal strain.

Zhenghao Liu obtained his BE degree in materials physics from Inner Mongolia University of Technology in 2013, and now he is a master degree candidate in the School of Materials Science and Engineering from Shijiazhuang Tiedao University. He is interested in performing quantum dots sensitized solar cells.

Jinxi Liu received his BE degree in engineering mechanics in 1982 from Liaoning University of Engineering Technology, Fuxin, China, and his MS and PhD degrees in 1988 and 1997 from Harbin Institute of Technology. He was a visiting professor at the Department of Mechanical Engineering of the University of Hong Kong under Croucher Foundation from 2000 to 2001. He is now a professor at the Department of Engineering Mechanics, Shijiazhuang Tiedao University. His research interests are the mechanics problems of photovoltaic, piezoelectric and magneto-electric materials and structures.

铆钉$CuGaS_2$量子点对提高太阳电池光伏性能的研究

赵晋津[1,2,3†*], 刘正浩[1,3†], 唐浩[4], 贾春媚[1], 赵星宇[1], 薛峰[5], 魏丽玉[1,3], 孔国丽[1], 王晨[1], 刘金喜[1*]

摘要 三元I–III–VI族黄铜矿量子点作为太阳电池的敏化剂表现出优异的光学性质. 我们采用一步法将2–5纳米的三元黄铜矿$CuGaS_2$量子点铆钉在TiO_2纳米颗粒上, 不通过任何有机分子作为链接制备出了TiO_2@CGS复合材料. 研究发现量子点和染料TiO_2@$CuGaS_2$/N719共敏化太阳电池效率达到7.4%, 相对于单敏化染料太阳电池而言, 其电池效率提高了23%. $CuGaS_2$量子点铆钉在半导体纳米颗粒增强了共敏化太阳电池的光吸收能力、增加了电荷载流子数量, 促进了电子有效注入, 具有十分广阔的应用空间.